2D+Depth RF Localization via a Low-Cost Receiver

Tianyuan Du
University of Michigan
Ann Arbor, USA
alexdu@umich.edu

Yang-Hsi Su
University of Michigan
Ann Arbor, USA
devilsu@umich.edu

Alanson Sample
University of Michigan
Ann Arbor, USA
apsample@umich.edu

***Abstract*—The proliferation of mobile devices in consumer electronics, IoT, and healthcare sectors has sparked considerable interest in wireless localization. While antenna array systems have demonstrated promise for wireless localization, they often entail high costs, intricate system designs, lengthy integration periods, and specialized packet formats. This study employs a 16-element L-shaped antenna array paired with a 2-channel 2MHz receiver, utilizing affordable and readily available components to localize incoming packets. The proposed approach calculates the 2D Angle of Arrival (AoA) of incoming signals using a custom Phase Difference Matching (PDM) algorithm. Additionally, a non-parallel wave depth estimator infers depth information of the signal source by learning phase difference trends. The result shows the system achieves median AoA error of 2.53 degrees horizontally and 1.88 degrees vertically, with an average depth estimation error of 1.07 m. This approach demonstrates the potential for 3D wireless localization of commonly available RF devices, through an N-element 2D phased array paired with a cost-effective commodity receiver.**

***Index Terms*—AoA Estimation, Indoor Localization**

I. Introduction

Wireless localization is an emerging technology that empowers various location-based services. These services include indoor navigation [1], asset tracking [2], healthcare [4], [5], augmented reality [6], [7], and smart home applications [3]. Over time, researchers have developed different techniques to locate wireless devices, relying on factors such as Received Signal Strength Indicator (RSSI) [11], [12], Angle of Arrival (AoA) [13]–[15], [19], and Time Difference of Arrival (TDoA) [9], [10] of the RF signal. Striking the right balance between localization accuracy, complexity, cost, and compatibility with existing devices is a goal for both academia and industry.

Among these techniques, AoA strikes a middle ground by offering better localization results than RSSI while demanding less hardware precision compared to TDoA. AoA-based systems calculate the angle of incoming RF signals using phased antenna arrays. By analyzing the phase differences of the RF signal simultaneously received by separate antennas, the Radio Frequency (RF) signal's AoA can be determined. The more antennas the system has, the more accurate the AoA estimation is. However, challenges emerge as the number of antennas increases. In typical AoA measurement systems, each antenna requires a dedicated RF chain, which is all-time synchronized, significantly inflating the cost as the number of antennas in the array increases. To address this challenge, a high-speed RF switch is employed to connect multiple antennas sequentially to a single receiver channel [14], [18]. Nevertheless, as the receiver collects the RF signal from one antenna at a time, phase measurements from asynchronous samples can contain carrier frequency offsets (CFO) that affect AoA calculations. Existing solutions either require modifications to the packet structure or involve signal accumulation across multiple packets to provide a single AoA estimation [16]. Unfortunately, these approaches may not be compatible with existing consumer hardware or may slow down system response times. Additionally, achieving synchronization with the RF switch demands extra hardware and receiver modifications, adding to system costs and complexity. Lastly, attempts to perform 3D wireless device localization using AoA from a single receiver either suffer from limitations in lower accuracy or necessitate deploying multiple antenna arrays at various locations within the space, which can hinder system deployment and usability [15], [17].

This paper proposes a cost-effective solution utilizing affordable and readily available components to achieve precise 2D+ depth localization. The system comprises a 16-element antenna array with 2 RF multiplexers (mux), each switches through 8 antennas sequentially. The outputs of the two switches are connected to a 2-channel receiver operating at a 2MHz sampling rate, enabling the localization of existing, unmodified consumer devices such as smartphones. Notably, the RF switch timing is not synchronized with the RF receive chain, reducing overall costs and system complexity. After detecting, identifying the packet, and recovering the switch timing within the signal processing stage, the 2D Angle of Arrival (AoA) of the received packet is calculated with the Phase Differences Matching (PDM) algorithm. Additionally, depth information of the signal source is inferred using a non-parallel wave depth estimator, which learns the phase difference trends in the RF signals that deviate from the plane wave. The system attains a median 2D AoA error of 2.53 horizontally and 1.88 degrees vertically, accompanied by an average depth estimation error of 1.07 m.

This paper makes the following contributions:

- A system for 2D AoA localization with two switched antenna arrays
- An phase difference matching algorithm for 2D AoA calculation
- An non-parallel wave depth estimator to infer depth from received phase

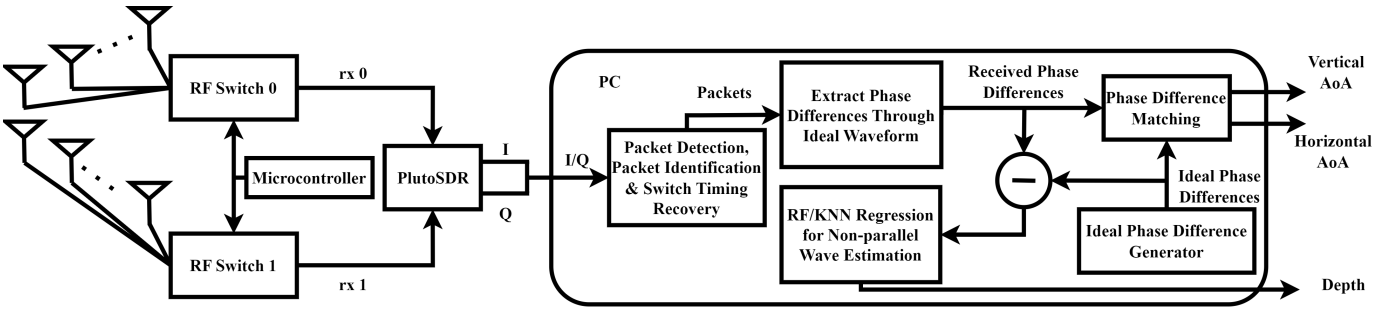

Fig. 1. The overall pipeline of the proposed system. The two RF multiplexers (mux) switch simultaneously controlled by a Teensy 4.0, and data are collected by a two-channel PlutoSDR, which are sent to a computer for processing. The signal processing pipeline includes packet detection and identification, switch timing recovery, phase difference extraction and ideal phase differences generation. Finally, Phase Difference Matching and non-parallel wave depth estimator are utilized to acquire 2D AoA and depth.

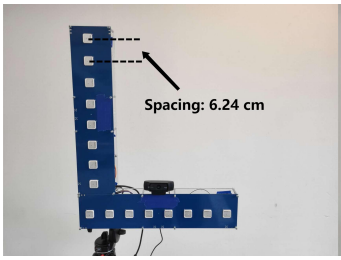

Fig. 2. Front View

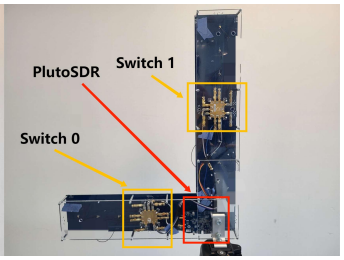

Fig. 3. Back View

Fig. 4. A picture of the L-shape antenna array. Each arm consists of 8 patch antennas. The spacing between the antennas is 6.24 cm, as half the wavelength of 2.402 GHz signals, and the center frequency of BLE advertising channel 37. On the back view of the antenna arrays, the positions of the switches are marked as yellow, and PlutoSDR is marked as red.

II. System Overview

This section outlines the system's hardware and signal processing flow, as shown in Fig 1. At the core of the antenna array is a PlutoSDR, a 2-channel Radio Frequency (RF) receiver operating at a 2MHz sampling rate. The device is budget-friendly as it operates on a single chip, and priced at approximately 230 dollars, it is over 80% cheaper compared to existing systems [13]. Each RF receive channel of the PlutoSDR connects to an 8:1 RF multiplexer (mux) that sequentially routes signals from eight antennas to the receiver, resulting in a 16 element antenna array. A Teensy 4.0 microcontroller is used to control the two RF switches simultaneously. This microcontroller operates independently from the receiver, following a predefined pattern to reduce extra hardware complexity and costs associated with synchronization. Importantly, previous research by Su et al. has demonstrated the potential to recover switch timing using a similar low-cost radio hardware architecture [18]. The two 8-element arrays from the two receiving channels are combined into a single 16-element array, as depicted in Fig 4. Data collected from the receiver is then transmitted to a computer for signal processing via a USB cable.

The software processing pipeline consists of multiple stages, as depicted in Fig 1. Initially, the system detects and identifies valid packets from the incoming data stream. Subsequently, it recovers the microcontroller's switch timing by observing discontinuities in the received waveform. Once a packet is identified, an ideal version of the packet waveform is generated in software and used as a virtual reference waveform to determine phase differences between each antenna. The Phase Difference Matching (PDM) algorithm is then used to calculate the 2D Angle of Arrival (AoA) by comparing these phase differences with the ideal phase differences corresponding to each 2D angle. Finally, a depth estimation algorithm takes into account the non-ideal characteristics of incoming radio waves, which are not parallel, to estimate the depth of the signal source. Subsequent sections provide a more detailed explanation of each of these steps.

III. Methods and Algorithms

This section dives into the three essential signal processing blocks in Fig 1, including *Packet Detection and Switch Timing Recovery*, Angle of Arrival (AoA) calculation with the *Phase Differences Matching Algorithm*, and the *Non-Parallel Wave estimator* for depth estimation and ultimately 3D receiver localization.

A. Packet Detection, Identification, and Switching Timing Recovery

The BLE advertising packets transmitted from the target device are embedded in the received data stream. Since the antenna array is switching while receiving, the sudden change from one antenna to another introduces discontinuities in the waveform, causing bit errors when detecting and decoding packets. Existing approaches [18] showed that iBeacon type advertising packets can be detected and identified based on their distinct properties. Specifically, iBeacon advertising packets from different devices are different solely in their Media Access Control (MAC) address, Universally Unique Identifier (UUID), and Cyclic Redundancy Check (CRC). Packet detection is accomplished through the computation of correlation scores between the received phase derivative of a received waveform segment, and the phase derivative of an ideal iBeacon waveform, which is generated from Matlab's BLE Toolbox. When the correlation score surpasses a preset threshold, which is established empirically at 0.5, the presence

of an iBeacon packet is confirmed. Subsequently, the packet is decoded, and the UUID is compared to a list of target UUID to identify whether the packet comes from any of the target devices.

After packets are detected and identified, received phases are matched to their corresponding antennas. In contrast to prior research, the receive chain operates asynchronously with the RF switch, resulting in a lack of knowledge regarding the assignment of data segments in the received signal to specific antennas [14]. To resolve this limitation, the system obtains switch timing by utilizing the discontinuity of the waveform. In this system, the microcontroller controls the RF switch in a pre-defined and continually repeating pattern, with a switching frequency of around 33.3 kHz. The duration of a BLE advertising packet is approximately 0.37 ms, which would allow approximately 12.3 switch events within the packet duration. Switching the receiving antenna from one to another in the middle of receiving a packet creates jumps and spikes in the received magnitude and phase derivative waveform. The pre-defined switching pattern sets a unique sampling duration on each antenna, so when it is matched to the phase derivative segments in the received single-channel waveform, antenna assignment could be recovered. The packet detection, identification and antenna matching pipeline has proven to be effective in previous work of Su et al [18].

B. Phase Difference Matching

This section presents the Phase Difference Matching (PDM) algorithm, a custom method that enables 2D AoA calculation by matching ideal phase differences with the received phase differences. This algorithm exemplifies the cooperative use of vertically and horizontally placed antenna arrays to simultaneously determine the vertical and horizontal angles of arrival.

The PDM Algorithm comprises the preprocess phase and the runtime phase, where the preprocess phase consists of multiple distinct steps. Initially, ideal phase offsets are constructed for all possible antenna pairs, based on two AoAs: $AoA_{horizontal}$ in the x-z plane and $AoA_{vertical}$ in the y-z plane, both ranging from -90 degrees to 90 degrees, as presented in Fig 5. This step accommodates all potential AoA scenarios and are executed before AoA measurements, which are in the runtime phase. Once $AoA_{horizontal}$ and $AoA_{vertical}$ are determined, the ideal phases of all 16 antennas are calculated, followed by the 16 phase differences between an arbitrarily determined null-antenna and every individual antenna. This involves converting $AoA_{horizontal}$ and $AoA_{vertical}$ into spherical coordinates ϕ and θ using the following mappings:

$$\theta = AoA_{horizontal} \tag{1}$$

$$\phi = \cot^{-1}\left(\sin\theta \tan AoA_{vertical}\right) \tag{2}$$

The positional relationship of θ, ϕ, $AoA_{horizontal}$ and $AoA_{vertical}$ are demonstrated in Fig 5.

Subsequently, the distance differences between each antenna with the null antenna could be computed based on θ, ϕ and their coordinates. Suppose the null-antenna located at

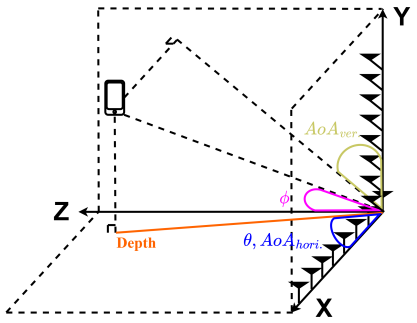

Fig. 5. Visual representation of the mapping from spherical angles to AoA described in Equation (1) and Equation (2). In practice, separately solving for the AoA on both antennas results in θ and the complementary angle of ϕ. To transform spherical angles to angles on the X-Z and Y-Z planes (horizontal and vertical AoA), previously mentioned equations are needed to construct the mapping.

(x_0, y_0, z_0), the phase difference between the null-antenna and another antenna at position (x_p, y_p, z_p) could be calculated by

$$d = \sqrt{(x_0 - x_p)^2 + (y_0 - y_p)^2 + (z_0 - z_p)^2} \tag{3}$$

$$\Delta\hat{\psi}_p = 2\pi\left(\frac{d\cos\theta}{\lambda\cos\phi} - k\right) - \pi, p = 0, 1, 2, ...14, 15 \tag{4}$$

Where d implies the distance between the two antennas, $\Delta\hat{\psi}_p$ implies the estimated phase difference between antenna p and the null antenna, and λ implies wavelength of BLE signals. Notice that k implies aliasing effects, which happens when $d\cos\theta > \lambda\cos\phi$. To effectively remove aliasing, phase differences are shifted into the range of $-\pi$ to π. By iterating within the range in one-degree spacing ($-90°$ to $90°$) on both directions, the computation results in 181 by 181 vectors of 16 elements, each vector representing the ideal phase differences between an antenna and the null antenna. By this approach, the ideal phase differences cover a comprehensive range of spatial directions.

During runtime, the processing operations are executed on a per-packet basis. Each antenna receives a segment of a packet, and the phase differences of antenna pairs are retrieved by comparing to an ideal waveform generated from the MATLAB BLE Toolbox. After iterating through a total of 16 antennas and getting each antenna's phase difference with the predetermined null-antenna that was initially selected during the preprocessing phase, identical steps of alias removal are performed. The runtime phase difference retrieval method is proven to be valid in prior work [18].

Subsetquently, the vector of obtained phase differences is compared with the 181 by 181 vectors of ideal phase differences. The objective is to pinpoint the 16-element ideal vector that most closely matches the obtained phase differences vector, defined by the lowest mean absolute error (MAE) of their differences. Once this optimal vector is identified, the pair of its associated coordinates are extracted, which represents the estimated AoA (in degrees) in the horizontal and vertical directions respectively.

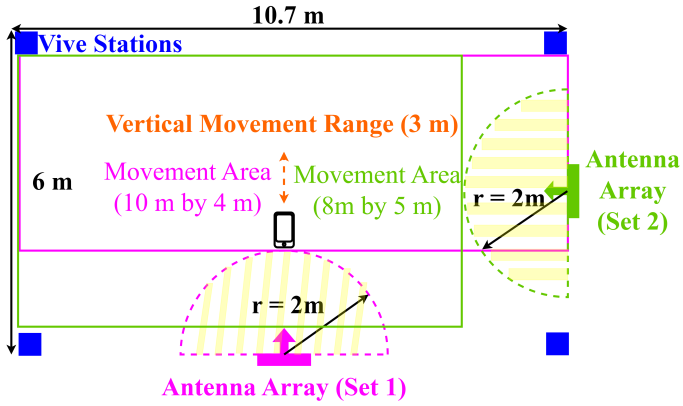

Fig. 6. A top-down view of the experiment setup. The designated area is 10.7 meters x 6 meters, with four vive base stations tracking a vive tracker for ground truth. A person holding a phone and a Vive tracker moves randomly within the purple area, and after the antenna position is changed, moves randomly within the green area.

C. Non-parallel Wave Depth Estimator

Taking the system's localization capabilities one step further from the confines of 2D Angle of Arrival (AoA) measurement, 3D localization could be enabled with depth information. The capability of 3D single-device RF localization with depth has been proven by prior work [15]. This research introduces a non-parallel wave depth estimator, an algorithm that achieves depth estimation of target devices with only phase information.

In the context of 2D AoA estimation using phase difference of arrival, a fundamental assumption is that waves propagate as planar wavefronts. However, waves emitted from a single source are not planar in real-world indoor applications, and by analyzing the differences in the received signals compared to a planar wavefront assumption, it is possible to coarsely estimate the depth of the source. Analytical approaches assuming spherical wavefronts are challenging using real-world signals since the deviations are low in amplitude and can be corrupted by environmental factors such as noise and RF multipath. To overcome this challenge, correlation between non-parallelism in waves and object depth is investigated through machine learning on features extracted by associating each set of received phase differences with their post-filtering AoA values. The machine learning models of choice in this work are the K-Nearest-Neighbor (KNN) Regressor and Random Forest (RF) Regressor for their low complexity and scalability.

The choice of model is motivated by the necessity for a regressor in this study to accommodate continuous data. To prevent overfitting, deep learning models are precluded from consideration. Regarding the two models of choice, KNN is chosen for its ability to approximate the association between variables and continuous outcome, and to infer new data from these approximates as a non-parametric method. Random Forest is chosen for its ensemble learning nature that suits well in handling noisy data with subtle features, which is characteristic of Radio Frequency data.

Upon each received vector of phase differences, identical preprocessing steps detailed in the preceding section are performed to generate ideal phase differences for the vertical and horizontal post-filtering AoA, as demonstrated in Equation (4). Subsequently, the inputs of machine learning pipelines are the differences between the received and the post-filtering estimated AoA's phase difference vectors, where the output is the estimated depth.

Considering the size of each dataset, KNN with K=500 and K=1000 are both examined, and the Random Forest Regressor contains 200 trees. Utilizing these machine learning models, depth estimation can be carried out using only phase information. Detailed experimental results are presented in the next section.

IV. Experiments and Evaluations

Two experiments are designed to evaluate the performance of the proposed method. The first experiment examines the 2D Angle of Arrival (AoA) accuracy, and the second experiment evaluates the depth estimation performance. The following sections introduces the experiment setup and the evaluation results. The evaluation used widely accepted matrices of mean absolute error (MAE) and median error [15], [18].

A. Experiment Setup

The area for experiments is a 10.7 m by 6 m area inside an indoor office space, denoted in Fig 6 and Fig 10. This area contains chairs, desks, and monitors that causes rich multipath, resembling real-world scenarios. Two experiments are designed and conducted with the purpose of assessing the system's effectiveness on measurement of 2D Angle of Arrival (AoA) and on depth estimation, respectively.

In both experimental scenarios, ground truth is retrieved using a Vive localization system with Vive Tracker 3.0, which was tracked by four base stations 2.0 positioned at the four corners of the experiment area, as demonstrated in Fig 6. Both experiments employed the same iPhone 7 as the target localization device. This choice of equipment was motivated by smartphones' wide availability in the real world.

The antenna locations and participant movement range are shown in Fig 6. During the experiment, a participant is invited to hold the Vive tracker closely to the iPhone and randomly

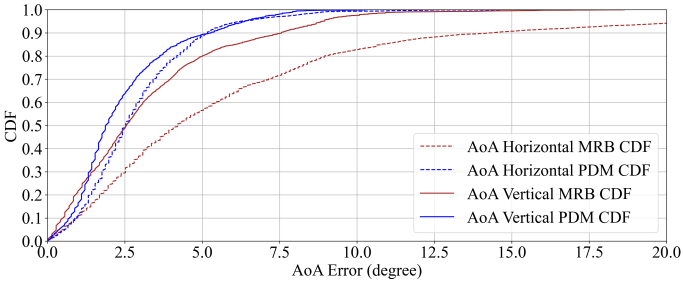

Fig. 7. Cumulative Distribution Function (CDF) of 2D AoA results. For the Phase Difference Matching algorithm, 90% of the AoA errors are less than 6 degrees on both vertical and horizontal AoA, an improvement on MRB, which reaches 8 degrees and 12 degrees on 90%.

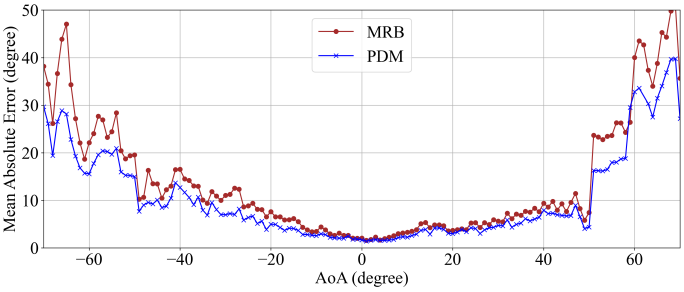

Fig. 8. Angle vs median error of horizontal AoA. From -30 to 30 degrees, PDM achieves error of less than 5 degrees, and within the range of -70 degrees to 70 degrees, PDM consistently outperforms MRB.

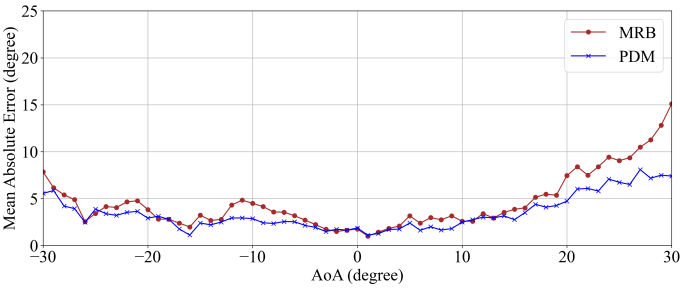

Fig. 9. Angle vs median error of vertical AoA. From -20 to 20 degrees, PDM achieves error of less than 5 degrees. It maintained its higher accuracy compared to MRB in the entire range of AoA, from -30 degrees to 30 degrees.

move in the designated area marked in Fig 6. In the first experiment, the participant moves in the purple area where the antenna array is put at the purple position, ranging 10 m by 4 m and height limit of 3 m. In the second experiment, the antenna array is put at the green location and the participant moves in the green area, ranging 8 m by 5 m and height limit of 3 m. For each random movement process, the participant is asked to walk and shift both the held objects up and down inside the designated test area for a continuous duration of 120 seconds, resulting in over 3000 to 3500 packets in one movement process. The random movements are done 5 times for the first experiment, and 5 times for the second experiment, consisting 16,352 and 14,218 data points respectively. Fig 10 demonstrates the real experiment setup, where the antenna array and Vive stations are explicitly marked out.

In subsequent passages, data from the first experiment is denoted as Set 1, and data from the second experiment is denoted as Set 2. The maximum range is 7.2 m and 7.9 m for Set 1 and Set 2 respectively.

B. Performance of Two-Dimensional AoA

Set 1 data are used to evaluate the effectiveness and accuracy of the Phase Difference Matching (PDM) algorithm. Performance of both horizontal and vertical are plotted in blue in Fig 8 and Fig 9, where the proposed system reaches median error of 2.53 degrees in horizontal AoA and 1.88 degress in vertical AoA. To provide comparison, results from Multi-Resolution Beaming (MRB) proposed by Su et al. is plotted in

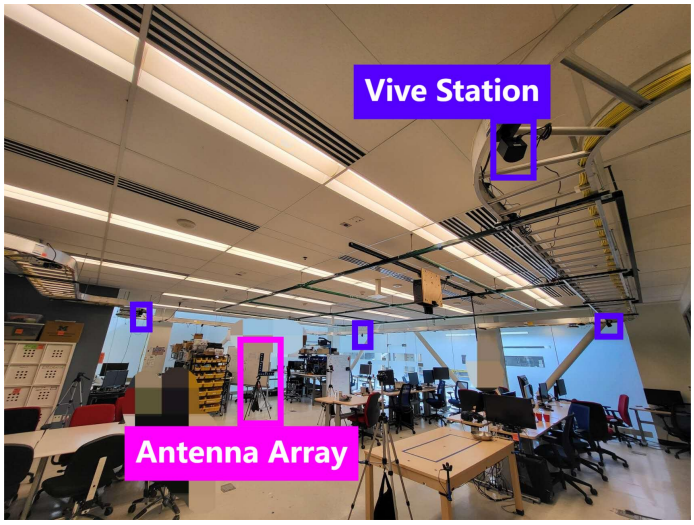

Fig. 10. The experiment environment as described in Fig 6. The Vive base stations are marked in blue and the antenna array is marked in purple. The office space has obstacles including desks, chairs, monitors etc. that creates multipath.

red on each corresponding plots [18]. MRB is considered valid as it also performs AoA measurements on BLE signals with switched antenna array, and they utilized comparable hardware as this work proposes in the sense of cost and complexity. Results show that PDM has a lower error than MRB across the entire scope of measurement, ranging from -70 degrees to 70 degrees horizontally and -30 degrees to 30 degrees vertically.

C. Performance of Depth Estimation

Data from both Set 1 and Set 2 are used to assess the system's effectiveness in performing depth estimation with the non-parallel wave depth estimator. Prior to applying machine learning on the collected data, both datasets go over a random shuffle. On each dataset, a 10 fold validation is performed. Cross dataset performance is also evaluated to test the system's robustness to environment changes. The proposed system reached an mean absolute error (MAE) of 0.86 m across a range of over 7 m on both within-dataset train-test splits and

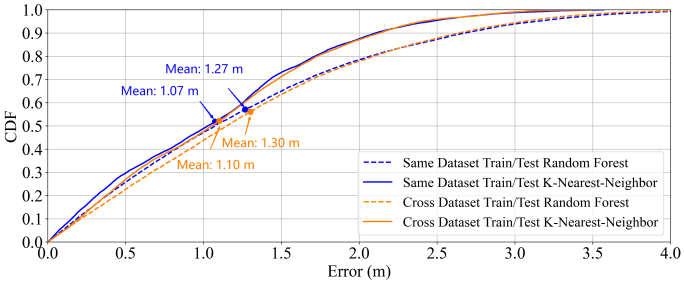

Fig. 11. Cumulative Distribution Function (CDF) of depth error for non-parallel wave depth estimator, where the mean values of each category is marked out. For the same dataset 10 fold validations, 90% of the errors are within 2.5 m. For cross dataset train-tests, 90% of the errors are within 3 m. Maximum depth of both datasets are over 7 m.

TABLE I
DEPTH ESTIMATION

	Median Error of Depth Estimation	
	Random Forest	KNN
Set 1 10-fold	1.04 m	0.86 m
Set 2 10-fold	1.27 m	1.14 m
Train/Test on Set 1/Set 2	1.20 m	1.21 m
Train/Test on Set 2/Set 1	1.10 m	0.86 m

cross-dataset train-test splits. Detailed results are shown in Fig 11, and median errors of all setup and model combinations are listed in table I.

Fig 11 showcases the overall performance of the non-parallel wave depth estimator. Results show that training and testing on fixed antenna array locations or different antenna array locations provide similar results, suggesting that the machine learning approach is valid in capturing depth information. The proposed system attains a median error of 0.86 m on cross-dataset trained and tested data. The results introduce a 23% improvement on the 1.06 m error proposed by prior research on 2D L-shape RF antenna array in multipath-prone environment [15].

V. CONCLUSION

In conclusion, this paper presents an affordable and practical solution for achieving 2D+depth indoor localization using low-cost, readily available components. The proposed system leverages a 16-element L-shape phased antenna array with two RF multiplexers, enabling 2D Angle of Arrival (AoA) localization without the need for mux-receiver synchronization. Through a custom Phase Difference Matching (PDM) algorithm and a machine-learning based non-parallel wave depth estimator to infer depth, the system achieves median AoA errors of 2.53 degrees horizontally and 1.88 degrees vertically, with an average depth estimation error of 1.07 meters. The proposed system demonstrates effectiveness in 2D+depth localization with a single locator, which has the potential to enable indoor localization applications with more accessible, low-cost components, hence providing new opportunities for the technology.

REFERENCES

[1] H. Zou, B. Huang, X. Lu, H. Jiang and L. Xie, "Standardizing location fingerprints across heterogeneous mobile devices for indoor localization," 2016 IEEE Wireless Communications and Networking Conference, Doha, Qatar, 2016, pp. 1-6, doi: 10.1109/WCNC.2016.7564800.

[2] C. K. M. Lee, C. M. Ip, T. Park and S. Y. Chung, "A Bluetooth Location-based Indoor Positioning System for Asset Tracking in Warehouse," 2019 IEEE International Conference on Industrial Engineering and Engineering Management (IEEM), Macao, China, 2019, pp. 1408-1412, doi: 10.1109/IEEM44572.2019.8978639.

[3] Z. Turgut, G. Z. G. Aydin, and A. Sertbas, "Indoor localization techniques for smart building environment," Procedia computer science, vol. 83, pp. 1176–1181, 2016.

[4] Alberto Alvarez-Alvarez, Jose M. Alonso, and Gracian Trivino. 2013. Human activity recognition in indoor environments by means of fusing information extracted from intensity of WiFi signal and accelerations. Information Sciences 233 (2013), 162 – 182. https://doi.org/10.1016/j.ins.2013.01.029

[5] P. Barsocchi, S. Chessa, F. Furfari, and F. Potortì. 2013. Evaluating Ambient Assisted Living Solutions: The Localization Competition. IEEE Pervasive Computing 12, 4 (2013), 72–79.

[6] Luca Calderoni, Matteo Ferrara, Annalisa Franco, and Dario Maio. 2015. Indoor localization in a hospital environment using Random Forest classifiers. Expert Systems with Applications 42, 1 (2015), 125 – 134. https://doi.org/10.1016/j.eswa.2014.07.042

[7] Buti Al Delail, Luis Weruaga, M. Jamal Zemerly, and Jason W. P. Ng. 2013. Indoor localization and navigation using smartphones augmented reality and inertial tracking. In 2013 IEEE 20th International Conference on Electronics, Circuits, and Systems (ICECS). 929–932. https://doi.org/10.1109/ICECS.2013.6815564

[8] Steven J. Henderson and Steven Feiner. 2009. Evaluating the benefits of augmented reality for task localization in maintenance of an armored personnel carrier turret. In 2009 8th IEEE International Symposium on Mixed and Augmented Reality. 135–144. https://doi.org/10.1109/ISMAR.2009.5336486

[9] Manikanta Kotaru, Kiran Joshi, Dinesh Bharadia, and Sachin Katti. 2015. SpotFi: Decimeter Level Localization Using WiFi. In Proceedings of the 2015 ACM Conference on Special Interest Group on Data Communication (London, United Kingdom) (SIGCOMM '15). Association for Computing Machinery, New York, NY, USA, 269–282. https://doi.org/10.1145/2785956.2787487

[10] Ahmed Makki, Abubakr Siddig, Mohamed Saad, Joseph R Cavallaro, and Chris J Bleakley. 2015. Indoor localization using 802.11 time differences of arrival. IEEE Transactions on Instrumentation and Measurement 65, 3 (2015), 614–623.

[11] Yiran Peng, Wentao Fan, Xin Dong, and Xing Zhang. 2016. An iterative weighted KNN (IW-KNN) based indoor localization method in bluetooth low energy (BLE) environment. In 2016 Intl IEEE Conferences on Ubiquitous Intelligence and Computing, Advanced and Trusted Computing, Scalable Computing and Communications, Cloud & Big Data Computing, Internet of People, and Smart World Congress (UIC/ATC/ScalCom/CBDCom/IoP/SmartWorld). IEEE, 794–800.

[12] Kanyanee Phutcharoen, Monchai Chamchoy, and Pichaya Supanakoon. 2020. Accuracy Study of Indoor Positioning with Bluetooth Low Energy Beacons. In 2020 Joint International Conference on Digital Arts, Media and Technology with ECTI Northern Section Conference on Electrical, Electronics, Computer and Telecommunications Engineering (ECTI DAMT & NCON). IEEE, 24–27

[13] K. Honda, D. Iwamoto and K. Ogawa, "Angle of arrival estimation embedded in a circular phased array 4 × 4 MIMO antenna," 2017 IEEE Asia Pacific Microwave Conference (APMC), Kuala Lumpur, Malaysia, 2017, pp. 93-96, doi: 10.1109/APMC.2017.8251385.

[14] Zhihao Gu, Taiwei He, Junwei Yin, Yuedong Xu, and Jun Wu. 2021. TyrLoc: a low-cost multi-technology MIMO localization system with a single RF chain. In Proceedings of the 19th Annual International Conference on Mobile Systems, Applications, and Services. 228–240.

[15] L. Zhang and H. Wang, "3D-WiFi: 3D Localization With Commodity WiFi," in IEEE Sensors Journal, vol. 19, no. 13, pp. 5141-5152, 1 July1, 2019, doi: 10.1109/JSEN.2019.2900511.

[16] Marco Cominelli, Paul Patras, and Francesco Gringoli. 2019. Dead on Arrival: An Empirical Study of The Bluetooth 5.1 Positioning System. In Proceedings of the 13th International Workshop on Wireless Network Testbeds, Experimental Evaluation amp; Characterization (Los Cabos, Mexico) (WiNTECH '19). Association for Computing Machinery, New York, NY, USA, 13–20. https://doi.org/10.1145/3349623.3355475

[17] E. Sippel, M. Lipka, J. Geiß, M. Hehn and M. Vossiek, "In-Situ Calibration of Antenna Arrays Within Wireless Locating Systems," in IEEE Transactions on Antennas and Propagation, vol. 68, no. 4, pp. 2832-2841, April 2020, doi: 10.1109/TAP.2019.2955147.

[18] Yang-Hsi Su, Chouchang Jack Yang, Euiseok Hwang, and Alanson P. Sample. 2023. Single Packet, Single Channel, Switched Antenna Array for RF Localization. Proc. ACM Interact. Mob. Wearable Ubiquitous Technol. 7, 2, Article 76 (June 2023), 25 pages. https://doi.org/10.1145/3596263

[19] P. Sambu and M. Won, "An Experimental Study on Direction Finding of Bluetooth 5.1: Indoor vs Outdoor," 2022 IEEE Wireless Communications and Networking Conference (WCNC), Austin, TX, USA, 2022, pp. 1934-1939, doi: 10.1109/WCNC51071.2022.9771930.